ARTICLE

Check for updates

Orthogonal antiferromagnetism to canted ferromagnetism in $CaCo_3Ti_4O_{12}$ quadruple perovskite driven by underlying kagome lattices

Midori Amano Patino [1], Fabio Denis Romero [1,2✉], Hyun-Joo Koo[3✉], Maxim Avdeev [4,5], Sean D. A. Injac[1], Masato Goto[1], Myung-Hwan Whangbo[3,6] & Yuichi Shimakawa [1✉]

$AA'_3B_4O_{12}$ quadruple perovskites, with magnetic A' and non-magnetic B cations, are characterized by a wide range of complex magnetic structures. These are due to a variety of competing spin-exchange interactions up to the fourth nearest neighbours. Here, we synthesize and characterize the magnetic behaviour of the $CaCo_3Ti_4O_{12}$ quadruple perovskite. We find that in the absence of an external magnetic field, the system undergoes antiferromagnetic ordering at 9.3 K. This magnetic structure consists of three interpenetrating mutually orthogonal magnetic sublattices. Under an applied magnetic field, this antiferromagnetic structure evolves into a canted ferromagnetic structure. In explaining these magnetic structures, as well as the seemingly unrelated magnetic structures found in other quadruple perovskites, we suggest a crucial role played by the underlying kagome lattices in these systems. All observed magnetic structures of these materials represent indeed one of the three possible ways to reduce spin frustration in the A' site kagome layers. More specifically, our survey of the magnetic structures observed for quadruple perovskites $AA'_3B_4O_{12}$ reveals the following three ways to reduce spin frustration, namely to make each layer ferromagnetic, to adopt a compromise 120° spin arrangement in each layer, or to have a magnetic structure with a vanishing sum of all second nearest-neighbour spin exchanges.

[1] Institute for Chemical Research Kyoto University, Gokasho, 611-0011 Uji, Japan. [2] Institut Néel Centre National de Recherche Scientifique, 25 Avenue des Martyrs, 38000 Grenoble, France. [3] Department of Chemistry and Research Institute for Basic Sciences Kyung Hee University, Seoul 02447, Republic of Korea. [4] Australian Nuclear Science and Technology Organization New Illawarra Rd, Lucas Heights, NSW 2234, Australia. [5] School of Chemistry The University of Sydney, Sydney, NSW 2006, Australia. [6] Department of Chemistry North Carolina State University, Raleigh, NC 27695-8204, USA. ✉email: fabio.denis-romero@neel.cnrs.fr; hjkoo@khu.ac.kr; shimak@scl.kyoto-u.ac.jp

xide materials adopting the perovskite structure show a wide range of physical, magnetic, and chemical properties as a consequence of the wide chemical flexibility of these materials[1]. This chemical flexibility is in part due to the ability of the network of corner-sharing octahedra in this structure to distort via twists and tilts to accommodate a wide range of cation sizes.

Of particular interest is the structure resulting from the $a^+a^+a^+$ tilt system, which produces the so-called quadruple perovskite structure shown in Fig. 1a[2]. This has the general formula $AA'_3B_4O_{12}$, where the A' site in materials adopting this structure type is of the appropriate size to host transition metal cations in square-planar coordination.

In materials with magnetic A' and non-magnetic B cations, there are a range of competing interactions between the orthogonally arranged square-planar A' sites that produce a wide variety of interesting emergent behaviour[3–10]. For instance, both $S = 1/2$ Cu^{2+} in $CaCu_3Ti_4O_{12}$ and $S = 2$ Mn^{3+} in $YMn_3Al_4O_{12}$ exhibit long-range antiferromagnetic (AFM) ordering with $T_N = 25$ and 35 K respectively[3,4]. In contrast, $S = 1/2$ Cu^{2+} spins in $CaCu_3Sn_4O_{12}$ and $CaCu_3Ge_4O_{12}$ order ferromagnetically (FM)[11]. $LaMn_3V_4O_{12}$ with $S = 5/2$ Mn^{2+} shows a symmetry-breaking magnetic structure below $T_N = 44$ K in which the spins on neighbouring Mn sites are arranged at 60° to each other in planes perpendicular to the [111] direction[7]. $CaCo_3V_4O_{12}$ shows collinear ordering of all $S = 3/2$ Co^{2+} spins ($T_N = 98$ K), but arranged in two sublattices along two separate k-vectors[8,9]. It is noted that the B cations of $LaMn_3V^{3.75+}_4O_{12}$ and $CaCo_3V^{4+}_4O_{12}$ possess d-electrons, but they exhibit no magnetic moment likely due to the delocalization of these electrons[7–9]. We recently reported the magnetic characterization of $CaFe_3Ti_4O_{12}$ with $S = 2$ Fe^{2+} at the A' sites, which adopts an unusual AFM structure ($T_N = 2.8$ K) in which the moment direction depends on the orientation of the FeO_4 square plane[10]. The resulting arrangement consists of three interpenetrating sublattices each made up of the set
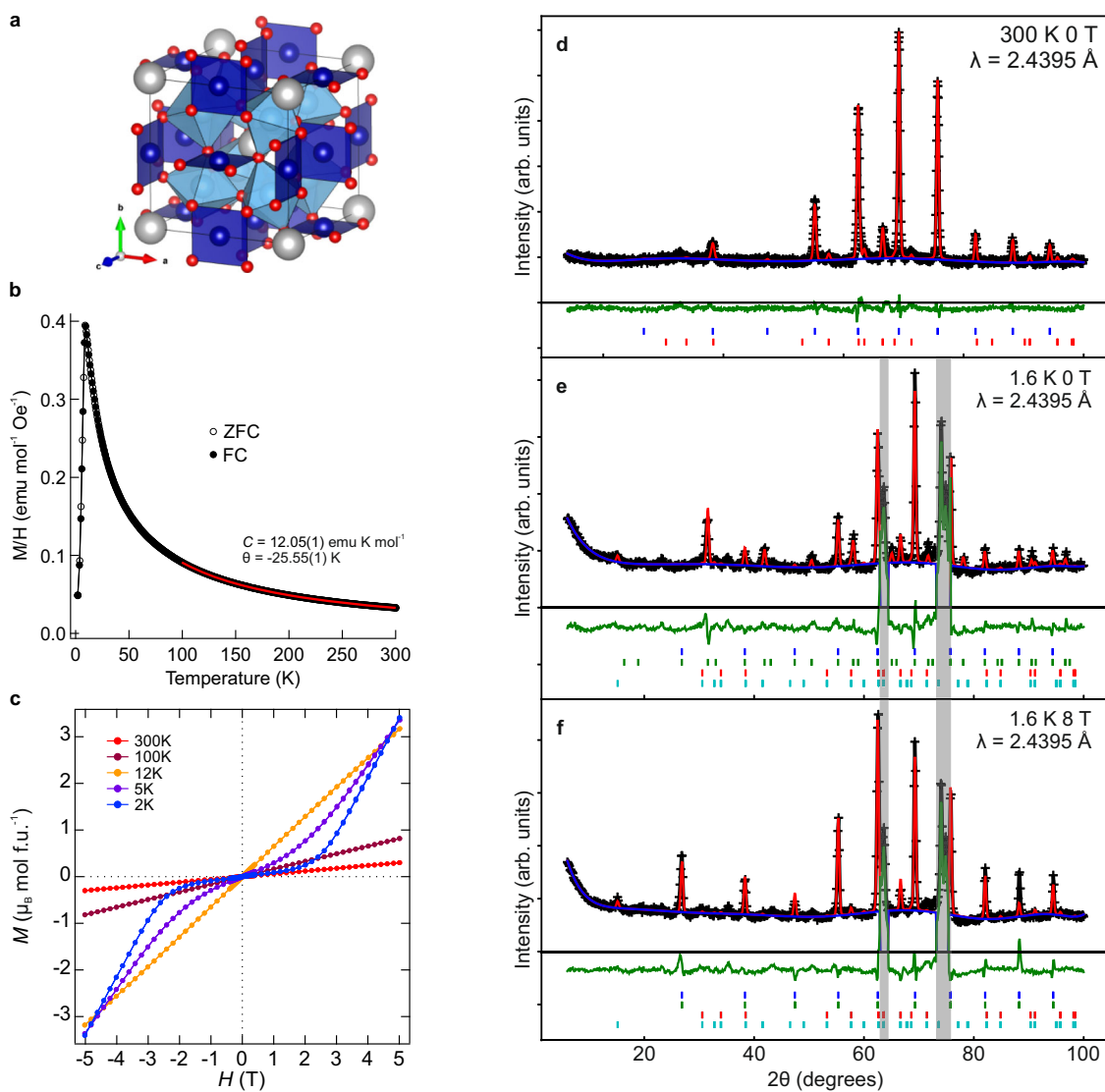

Fig. 1 Crystal structure and experimental data collected from CaCo₃Ti₄O₁₂. a Quadruple perovskite crystal structure. **b** Zero-field (ZFC) and field cooled (FC) magnetization data collected as a function of temperature from $CaCo_3Ti_4O_{12}$ under an applied field of 1 T. **c** Magnetization data collected as a function of field from $CaCo_3Ti_4O_{12}$. Observed (black), calculated (red), and difference (green) plots from the refinement of $CaCo_3Ti_4O_{12}$ against neutron powder diffraction data collected at **d** 300 K, **e** 1.6 K under 0 T, and **f** 1.6 K under 8 T. In **d** the upper set of tick marks corresponds to contributions from $CaCo_3Ti_4O_{12}$ and the lower set to contributions from the $CoTiO_3$ secondary phase. In **e** and **f** from top to bottom the tick marks correspond to: $CaCo_3Ti_4O_{12}$ nuclear and magnetic reflections and $CoTiO_3$ nuclear and magnetic reflections. The shaded regions correspond to contributions from the cryomagnet which were excluded from the refinement.

of square planes sharing a common orientation. Under high applied magnetic field, $CaFe_3Ti_4O_{12}$ displays metamagnetic behaviour. Its magnetic structure switches to a canted FM state consisting of three FM sublattices (cFM phase)[10].

Understanding the behaviour of these materials is complicated by a wide range of properties exhibited and a large number of competing interactions and electronic effects including Coulomb correlations, spin-orbit coupling, and orbital polarization. It is clear that first and second nearest neighbour (1NN and 2NN, respectively) interactions are not sufficient to explain the observed behaviour in these materials, and we must consider third and fourth neighbour spin exchanges (3NN and 4NN, respectively).

In this work, we prepare and characterize the quadruple perovskite $CaCo_3Ti_4O_{12}$ with Co^{2+} ($S = 3/2$) cations occupying the A' sites, to find that it adopts an orthogonal magnetic structure similar to that observed for $CaFe_3Ti_4O_{12}$ with some key differences. We carry out DFT+U and DFT+U+SOC calculations to analyze the magnetic structure of $CaCo_3Ti_4O_{12}$. We show that various magnetic structures of quadruple perovskites are readily explained from the viewpoint of avoiding spin frustration in the underlying kagome spin lattices of their A' cations.

Results and discussion

Initial characterization. Laboratory X-ray powder diffraction data collected from the products of reaction between $CaTiO_3$ and $CoTiO_3$ at 1600 °C and 13.5 GPa were consistent with the formation of a phase adopting the quadruple perovskite structure shown in Fig. 1a. A model based on the quadruple perovskite structure was refined against synchrotron X-ray powder diffraction data and produced excellent statistical and observed fits, confirming the material crystallizes in a cubic structure (space group $Im-3$) with a lattice parameter $a = 7.4398(1)$ Å. Observed, calculated, and difference plots are shown in Supplementary Fig. 1a and the refined structural parameters are given in Supplementary Table 1.

Zero-field (ZFC) and field cooled (FC) magnetization data were collected from a sample under an applied field of 1 T and are shown in Fig. 1b. These contain a local maximum at $T = 9.3$ K consistent with an AFM transition. A fit of the ZFC data to the Curie–Weiss law ($\chi = C/(T-\theta)$) in the region $100 \leq T$ (K) ≤ 300 yields values of $C = 12.05(1)$ emu K mol^{-1} and $\theta = -25.55(1)$ K. The calculated Curie constant yields an effective moment of $\mu_{eff} = 5.67(1)$ μ_B consistent with high-spin $S = 3/2$ Co^{2+}, for which the theoretical spin-only moment would yield 3.87 μ_B. The higher-than-expected moment indicates the presence of an orbital contribution to the paramagnetic moment. Magnetization data collected above 10 K are linear through the origin. However, data collected at 2 K show an unusual shape consistent with metamagnetic behaviour with a transition at $H_C \approx 2.5$ T Fig. 1c.

A model based on the quadruple perovskite structure could be refined against neutron powder diffraction data collected at 300 K to yield excellent calculated and observed fits. Plots of the refinement are shown in Supplementary Fig. 1b and the refined structural parameters are given in Supplementary Table 2. A small amount of $CoTiO_3$ (8.8% by weight) was included as a secondary phase. No antisite disorder was observed when the cation site occupancies were allowed to refine. Bond valence sums calculated from the refined structure yielded values of 1.849, 1.704, and 4.093 for Ca, Co, and Ti, respectively, confirming the composition as $CaCo^{2+}_3Ti^{4+}_4O_{12}$[12]. The obtained compound thus contains magnetic Co^{2+} ions at the A' site and nonmagnetic Ti^{4+} ions at the B site.

Zero-field magnetic structure. Low temperature neutron powder diffraction data were collected from $CaCo_3Ti_4O_{12}$ at 1.6 K under

zero field. These data contained additional reflections consistent with long-range magnetic order. All the magnetic reflections which did not originate from the $CoTiO_3$ impurity could be indexed on the basis of a magnetic cell with a propagation vector $k = (\frac{1}{2}, \frac{1}{2}, \frac{1}{2})$ on the basis of the nuclear cell. This magnetic propagation vector is different from that found in $CaFe_3Ti_4O_{12}$ ($k = (\frac{1}{2}, \frac{1}{2}, 0)$), indicating an overall different arrangement of magnetic moments in the two materials[10]. The highest symmetry magnetic structure (space group F_S23), which correctly accounted for the peak intensities, is shown in Fig. 2a.

This structure consists of three interpenetrating magnetic sublattices corresponding to sets of CoO_4 square planes sharing a common orientation. It contains two different inequivalent Co sites, which were constrained to have the same moment M, allowing the structure to be refined using a single parameter ($|M|$). The refinement produced excellent calculated ($\chi^2 = 7.52$) and observed fits (Fig. 1e) and resulted in a refined moment of 3.76 μ_B per Co centre. Full details of the refined structural model are given in Supplementary Table 3.

Under no applied magnetic field, $CaCo_3Ti_4O_{12}$ exhibits long range magnetic ordering with a transition temperature $T_N = 9.3$ K. The refined magnetic structure contains similarities to that observed previously in $CaFe_3Ti_4O_{12}$ ($T_N = 2.3$ K)[10]. Both structures consist of three mutually orthogonal AFM sublattices, each of which corresponds to the set of MO_4 square planes that share a common orientation (Fig. 2a). The difference between the two structures lies in the sign of one of the 4NN interactions between parallel MO_4 square planes. In the magnetic structure of $CaCo_3Ti_4O_{12}$, all three 4NN interactions are AFM while in $CaFe_3Ti_4O_{12}$ one of them ($J_4(\pi Ca)$, see below) is FM, resulting in the two different observed magnetic structures[10].

High-field magnetic structure. Neutron powder diffraction data collected from $CaCo_3Ti_4O_{12}$ at 1.6 K and under an applied magnetic field of 8 T did not contain the magnetic reflections present in the data collected at 0 T, but did contain additional reflections relative to the data collected at 300 K. These could be indexed using a magnetic propagation vector $k = (0, 0, 0)$. A model in which all Co moments are collinear could not account for the observed magnetic intensities. The $R-3$ model previously proposed for $CaFe_3Ti_4O_{12}$ at fields $H \geq 0.25$ T (shown in Fig. 2b) was found to be compatible with the data[10]. This was refined against the data to yield good calculated ($\chi^2 = 8.95$) and observed fits and yielded a moment of 3.04(1) μ_B per Co centre. Plots of the data are shown in Fig. 1f and refined parameters are given in Supplementary Table 4. However, a complete characterization of field-stabilized magnetic structure requires taking into account domain population and is better done on a single crystal.

Neutron powder diffraction data collected under applied fields $H \geq 2.5$ T show a gradual suppression of the magnetic reflections originating from the AFM structure and the emergence of different magnetic reflections (Supplementary Fig. 2).

As in the AFM case, the magnetic structure of $CaCo_3Ti_4O_{12}$ under a high magnetic field consists of three sublattices that correspond to the square plane orientations (Fig. 2b, left). Within each sublattice, all moments are collinear and ferromagnetically ordered. However, the spins of all three FM sublattices are not collinear so as to reduce the magnetic dipole–dipole (MDD) interactions[13–15].

Spin exchanges. In order to understand the zero-field (F_S23) AFM structure of $CaCo_3Ti_4O_{12}$, we first consider Heisenberg (isotropic) spin exchange. The energy between two spins i and j is described by the Heisenberg exchange energy, $-J_{ij}\left(S_i \cdot S_j\right)$[15–17]. This energy vanishes for each 1NN exchange because the two
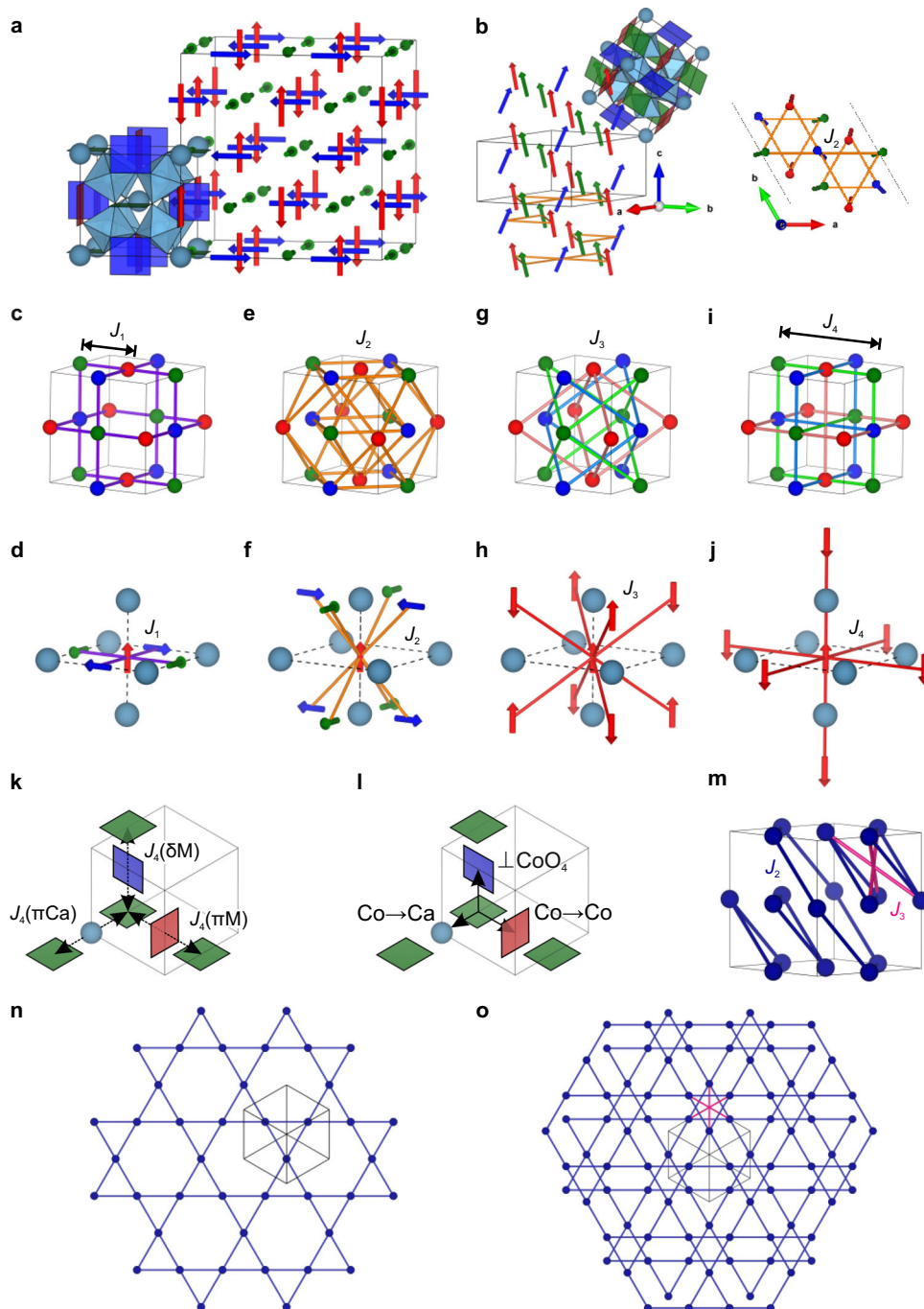
Fig. 2 Magnetic structures of CaCo₃Ti₄O₁₂ and spin interactions in quadruple perovskites. Refined magnetic structures of $CaCo_3Ti_4O_{12}$ at 1.6 K and under **a** 0 T and **b** 8 T. Red, blue, and green centres each correspond to a set of CoO_4 square planes sharing a common orientation. **c** J_1 exchange between 1NN. **d** Relative arrangement of 1NN centres in the 0 T magnetic structure of $CaCo_3Ti_4O_{12}$. **e** J_2 exchange between 2NN. **f** Relative arrangement of 2NN centres. **g** J_3 exchange between 3NN. **h** Relative arrangement of 3NN centres. **i** J_4 exchange between 4NN. **j** Relative arrangement of 4NN centres. **k** Three different J_4 interactions. **l** Moment directions considered during DFT calculations (detailed in the Supplementary Fig. 4). **m** Arrangement of the kagome layers along the [111] direction. **n** A kagome layer of J_2 spins perpendicular to [111]. **o** Projection view of two adjacent kagome layers of J_2 spins perpendicular to [111].

spins involved in the exchange path are orthogonal, resulting in $S_i \cdot S_j = 0$ (Fig. 2c, d). For the same reason, the exchange between 2NN also vanishes (Fig. 2e, f). The two spins in each 3NN are parallel and the exchange between these is therefore nonzero (Fig. 2g). However, in this structure, half of the 3NN paths have the spins ferromagnetically coupled, and the other half have the spins antiferromagnetically coupled (Fig. 2h). Thus, the sum of

3NN spin exchanges vanishes in this structure. That is to say, the AFM arrangement is not determined by 1NN, 2NN, or 3NN spin exchanges.

In cases when Heisenberg exchange fails to account for observed magnetic properties, it is common to consider Dzyaloshinskii-Moriya (DM, asymmetric) exchange between spin sites given by $-D_{ij} \cdot (S_i \times S_j)$[15–18]. This exchange is typically an

order of magnitude weaker than the corresponding Heisenberg spin exchange. In this structure, the DM term for each 1NN path is zero as these centres lie on two orthogonal mirror planes, and no DM vector can be perpendicular to both. For the 2NN exchange paths, the individual DM terms are not necessarily zero, but the sum total of them is zero. Thus, the DM interactions cannot be responsible for the observed arrangement.

This prompted us to examine 4NN interactions (Fig. 2i, j). There are three kinds of 4NN interactions to consider as shown in Fig. 2k:

$J_4(\delta M)$Between two MO_4 planar units parallel to each other along a direction normal to the planes with an intermediate orthogonally oriented MO_4 unit.

$J_4(\pi M)$Between two coplanar MO_4 units along a direction ∥ to these with an intermediate orthogonal MO_4 unit.

$J_4(\pi Ca)$Between two coplanar MO_4 units along a direction ∥ to these with an intermediate orthogonal Ca centre.

We evaluated the values of the 1NN, 2NN, and 3NN spin exchanges in $CaCo_3Ti_4O_{12}$ via energy mapping analysis based on first principles DFT calculations[15–17,19–23]. Details of these calculations are given in the Supplementary Note 6. The ordered spin states that were used are defined in Supplementary Fig. 4. Our DFT+U calculations for $CaCo_3Ti_4O_{12}$ show that $J_1 = 0.95$ K, $J_2 = -0.86$ K, and $J_3 = -0.64$ K using $U_{eff} = U - J = 4$ eV. Namely, J_1 is FM while J_2 and J_3 are AFM, but all these spin exchanges are very weak. As already mentioned, these exchanges do not determine the AFM magnetic structure. We note that there were DFT studies on $CaCu_3B_4O_{12}$ (B = Ti^{4+}, Ge^{4+}, Sn^{4+}) and $CaCo_3V_4O_{12}$[24,25].

We now examine the 4NN spin exchanges $J_4(\pi Ca)$, $J_4(\pi M)$, and $J_4(\delta M)$. To find how their values are affected by the orientation of the spins in each 4NN exchange path, we include spin-orbit coupling (SOC) in the DFT+U calculations. These DFT+U +SOC are simplified by employing the "dimer" model, in which all Co^{2+} ions except for those of the two CoO_4 square planes defining the 4NN spin exchange are replaced with nonmagnetic Zn^{2+} ions. Note that these correspond to the Co^{2+} ions located between the two CoO_4 square planes in $J_4(\pi M)$ and $J_4(\delta M)$. One needs to consider three different spin directions for the Co^{2+} ion of each CoO_4 square plane. One direction is perpendicular to the CoO_4 plane (⊥CoO_4). The in-plane spin orientation is not isotropic, so we distinguish two-moment directions: either parallel to the Co-Ca-Co direction (hereafter Co→Ca) or parallel to the Co-⊥Co-Co direction (hereafter Co→Co) (Fig. 2l and S4).

We examined AFM and FM arrangements for each combination of spin direction and 4NN exchange path. Our DFT+U +SOC calculations show that, for each spin orientation, the AFM coupling is more stable than the FM coupling in all three 4NN exchange paths. The relative energies calculated for the AFM states of each 4NN spin exchange path with three different spin orientations are summarized in Table 1. The results show that for each 4NN exchange path, the ∥CoO_4 orientations are more stable than the ⊥CoO_4 orientation. Furthermore, of the two ∥CoO_4

orientations, the one pointed along the Co→Ca direction is more stable as can be confirmed from the sum of the relative energies in Table 1. This is consistent with the experimentally observed magnetic structure.

We now calculate the values of $J_4(\pi Ca)$, $J_4(\pi M)$, and $J_4(\delta M)$ based on their most stable spin orientations. Given the energy difference $\Delta E = E_{AFM} - E_{FM} = JS^2$, where $S = 3/2$ for Co^{2+}. Thus, from the ΔE values calculated, we obtain $J_4(\pi Ca) = -3.9$ K, $J_4(\pi M) = -0.3$ K, and $J_4(\delta M) = -2.0$ K. All three 4NN spin exchanges are AFM with one particularly weak interaction. This is consistent with the fact that $CaCo_3Ti_4O_{12}$ undergoes an AFM ordering at a low temperature (i.e., $T_N = 9.3$ K).

Underlying kagome layers in quadruple perovskites. As described above, the AFM structure of $CaCo_3Ti_4O_{12}$ observed in the absence of external magnetic field is converted to the canted FM structure upon applying an external magnetic field. This is puzzling because the two magnetic structures appear quite unrelated. It is important to probe if the cause is hidden in plain view. We note that certain low-dimensional metals possessing several partially filled bands exhibit charge density wave instabilities although their individual Fermi surfaces do not show any observed nesting vectors. This puzzling observation is explained by the introducing concept of hidden Fermi surface nesting[26]. We now show that the magnetic ions Co^{2+} of $CaCo_3Ti_4O_{12}$ form kagome layers perpendicular to the [111] direction, and the spin frustration of these underlying kagome layers not only provides a natural connection between the AFM structure and the canted FM structure of $CaCo_3Ti_4O_{12}$, but also may explain the variety of spin structures observed in A'-site magnetic quadruple perovskites. Notably, the $Im\overline{3}$ cubic crystal structure of $CaCo_3Ti_4O_{12}$ provides perfect kagome lattices with no distortion. Each nuclear unit cell will contain four sets of kagome layers perpendicular to the four body diagonal directions. However, due to the cubic symmetry, all of these are equivalent, indistinguishable, and related by rotations. We therefore only need to consider one set of kagome layers.

We note that the 2NN paths J_2, when extended, consist of kagome layers stacked along the [111] direction (Fig. 2m, n). Adjacent kagome layers interact via the 3NN exchange J_3 make the hexagram arrangement using half the (J_2, J_2, J_2) triangles as depicted in Fig. 2m, o. These underlying kagome layers play an important role in determining the magnetic structures of quadruple perovskites $AA'_3B_4O_{12}$. The high-field magnetic structure can be described as resulting from FM kagome layers in which all spins are oriented along the [111] direction and the moments canted with respect to the three-fold rotational axis. The senses of the spin canting between the two adjacent (J_2, J_2, J_2) triangles, connected by the J_3 paths, are opposite such that the two spins in each J_3 path are parallel to each other. It is important to notice that 2NN spin exchanges do not take place between NN kagome layers, but between 2NN kagome layers (Fig. 2e), which plays an important role in the magnetic structures of other quadruple perovskites.

We now consider the spin frustration that would result from AFM J_2 interactions. The ordered magnetic structures of quadruple perovskites under zero applied field show three different ways to relieve this spin frustration. The first is to have FM coupling within each kagome layer (made up of J_2) and AFM coupling between layers (through J_3). This is the arrangement observed in $S = 1/2$ $CaCu_3Ti_4O_{12}$[3]. Because of the AFM J_3 paths, every second layer will have the same spin arrangement, minimizing the frustration of the (J_2, J_2, J_2) triangles between every second J_2-kagome layers (Fig. 2e). The second way to reduce spin frustration is to have a compromise 120° spin

Table 1 Calculated relative energies of CoO₄ dimers.

	∥CoO_4 Co→Ca[a]	∥CoO_4 Co→Co[a]	⊥CoO_4
$J_4(\pi Ca)$ path	0 [b]	19.4	47.3
$J_4(\pi M)$ path	0 [b]	19.7	47.8
$J_4(\delta M)$ path	19.4	0 [b]	47.6

[a]The orientation of the spins within the CoO₄ square planes.
[b]More stable than the FM state by 8.8 K for $J_4(\pi Ca)$, 0.6 K for $J_4(\pi M)$, and 4.6 K for $J_4(\delta M)$.
Spin orientation effect on the relative energies (in K per two Co atoms) of the antiferromagnetically-coupled CoO₄ dimers in the 4NN spin exchange paths. These energies were obtained from DFT+U+SOC calculations with $U_{eff} = 4$ eV.

arrangement. This is the situation observed in $LaMn_3V_4O_{12}$ with AFM coupling between adjacent layers[7].

The third way to reduce the spin frustration is to have a magnetic structure with a vanishing sum of all J_2 exchanges. The Co^{2+} ions in the AFM structure of $CaCo_3V_4O_{12}$ are divided into two interpenetrating sublattices, in each of which the (J_2, J_2, J_2) triangles have equal numbers of (↑↑↓) and (↑↓↓) spin arrangements so that the sum of all J_2 spin exchanges vanishes[9]. In $CaFe_3Ti_4O_{12}$ and $CaCo_3Ti_4O_{12}$, the magnetic arrangement consist of three inter-penetrating sublattices such that the spins on all J_2 paths are orthogonal to each other making the sum of all J_2 vanish[10].

A canted FM (i.e., cFM) structure observed for $CaFe_3Ti_4O_{12}$ and $CaCo_3Ti_4O_{12}$ under high-field (Fig. 2b) is a combination of two different ways of reducing the spin frustration in the underlying kagome layers; one is a FM arrangement with spins oriented along the [111] direction, and the other is a compromise 120° spin arrangement with spins oriented perpendicular to the [111] direction. The FM arrangement is brought about by the external magnetic field, and the collinear spins of this arrange-ment become canted by introducing the compromise 120° spin arrangement. This spin canting is energy-lowering because it reduces the extent of the MDD interactions that occur among the collinear spins in the FM arrangement[13–15]. In forming the cFM structure under high high-field, the spin exchanges J_2 and J_3, which are both are substantially AFM (Supplementary Table 7), play a major role. Under high-field, the spin moments are lined up with the field. Thus, when the spins are lined up along the [111] direction, the spins of each kagome lattice become ferromagnetically coupled leading to the collinear FM arrange-ment throughout the kagome lattices. This spin arrangement is energetically favourable in terms of avoiding spin frustration associated with the J_2 paths, but unfavourable in terms of MDD interactions. To reduce the latter, the spins of each kagome lattice cant by introducing a 120° compromise character such that the spins of the J_3-paths between adjacent kagome lattices are antiferromagnetically coupled to gain energy from the J_3 exchanges (Fig. 2m). This requires a "three-in" compromise arrangement in one spin triangle and a "three-out" compromise arrangement in the adjacent spin triangle (Fig. 2b). This explains why the canted spins are parallel in every second kagome lattices.

Conclusions

We prepared and characterized the quadruple perovskite $CaCo_3Ti_4O_{12}$ with $S = 3/2$ ions Co^{2+} at the square planar A' sites. This material orders antiferromagnetically at $T_N = 9.3$ K to adopt a magnetic structure consisting of three interpenetrating mutually orthogonal magnetic sublattices. Each sublattice is made up of CoO_4 square planes possessing a common spin orientation. The formation of this AFM structure is not determined by the 1NN, 2NN, and 3NN spin exchanges, nor by DM interactions, but by the 4NN spin exchanges as well as SOC. The latter makes all spins lie in the plane of the CoO_4 units along the Co→Ca direction. It is important to note that the magnetic ions A' of quadruple per-ovskites $AA'_3B_4O_{12}$, though cubic in structure, form kagome layers of 2NN spin exchange J_2 perpendicular to the [111] direction, and that minimization of spin frustration in the J_2-kagome layer is a common denominator for all different magnetic structures of $AA'_3B_4O_{12}$ in the absence and presence of external magnetic fields. There are three ways of relieving the spin frustration in these J_2-kagome layers; (1) to make each J_2-kagome layer FM, (2) to make J_2-kagome layer adopt a compromise 120° spin arrangement, or (3) to make the sum of all J_2 spin exchanges vanish. The first two ways are combined together in forming the canted FM structure of $CaCo_3Ti_4O_{12}$ and $CaFe_3Ti_4O_{12}$, which occurs to reduce the MDD interactions of the collinear spins in the pure FM structure.

Methods

Sample preparation. Samples of $CaCo_3Ti_4O_{12}$ were prepared from a 1:3 molar ratio of $CaTiO_3$ and $CoTiO_3$. $CaTiO_3$ was prepared from a mixture of $CaCO_3$ (99.5%) and TiO_2 (99.9%, dried at 900 °C) ground together using an agate mortar and pestle. The resulting powder was pressed into a pellet and fired at 1000 °C for 3 periods of 24 h with intermediate regrinding and repelletising steps. $CoTiO_3$ was prepared from a mixture of CoO (99.9%) and TiO_2 ground together, pelletised, and heated in a vacuum-sealed ampoule at 900 °C for 72 h.

The precursor mixture for $CaCo_3Ti_4O_{12}$ was ground together using an agate mortar and pestle and then ball milled using agate spheres for 2 h. The resulting powder was loaded into platinum capsules and treated at 1600 °C under 13.5 GPa for 1 h using a 6–8 cubic multianvil press. The pressure was released slowly after quenching to room temperature. In order to prepare a sufficient amount of material for neutron powder diffraction measurements, six samples (approx. 50 mg each) were prepared from a common precursor mixture. Laboratory X-ray diffraction data were collected using a Bruker D8 diffractometer and showed some of these contained a small amount of unreacted $CoTiO_3$ (<5% by mass). The sample containing the least amount of secondary phase was selected for magnetic and physical property measurements.

Diffraction experiments. Synchrotron X-ray powder diffraction data collected using the BL02-B2 beamline at Spring-8 synchrotron, Hyogo, Japan from a sample that did not show any peaks corresponding to unreacted precursors or unwanted secondary phases (shown in Supplementary Fig. 1a).

Neutron powder diffraction data were collected from a mixture of the products of five separate experimental runs using the ECHIDNA diffractometer at the OPAL reactor, Sydney, Australia[27]. These samples were ground together using an agate mortar and pestle and pressed into a 5 mm diameter pellet. The pellet was placed in a vanadium can and fixed in place using a cadmium rod. Data suitable for structural characterization were collected at 300 K using a wavelength of 1.6215 Å. Data at low temperatures were collected using a cryomagnet and a wavelength of 2.4395 Å. Rietveld analysis was carried out using GSAS-II[28]. Magnetic structure solutions were carried out using k-SUBGROUPSMAG as implemented in GSAS-II[28,29].

Magnetic property measurements. Magnetic property measurements were car-ried out using an MPMS-XL SQUID magnetometer.

DFT calculations. To determine the spin exchanges of $CaCo_3Ti_4O_{12}$, we carried out spin-polarized DFT+U calculations by using the frozen-core projector aug-mented plane wave (PAW) encoded in the Vienna ab Initio Simulation Package (VASP) and the PBE exchange-correlation functional[19–22]. The electron correlation associated with the 3d states of Co was taken into consideration by DFT+U calculations with an effective on-site repulsion $U_{eff} = U − J = 4$ and 5 eV[23]. All our DFT calculations used the plane wave cutoff energy of 450 eV, and the threshold of 10^{-6} eV for self-consistent-field energy convergence. We employed a set of $(8 × 8 × 8)$ k-points for DFT+U calculations and a set of $(4 × 4 × 4)$ k-points for DFT+U+SOC calculations[30].

References

1. George, G., Ede, S. R. & Luo, Z. *Fundamentals of Perovskite Oxides* (CRC Press, 2020).
2. Glazer, A. M. The classification of tilted octahedra in perovskites. *Acta Crystallogr. B Struct. Crystallogr. Cryst. Chem.* **28**, 3384–3392 (1972).
3. Kim, Y. J., Wakimoto, S., Shapiro, S. M., Gehring, P. M. & Ramirez, A. P. Neutron scattering study of antiferromagnetic order in $CaCu_3Ti_4O_{12}$. *Solid State Commun.* **121**, 625–629 (2002).
4. Tohyama, T., Saito, T., Mizumaki, M., Agui, A. & Shimakawa, Y. Antiferromagnetic interaction between A'-site Mn spins in A-site-ordered perovskite $YMn_3Al_4O_{12}$. *Inorg. Chem.* **49**, 2492–2495 (2010).
5. Shimakawa, Y. & Saito, T. A-site magnetism in A-site-ordered perovskite-structure oxides. *Phys. Status Solidi B* **249**, 423–434 (2012).
6. Toyoda, M., Saito, T., Yamauchi, K., Shimakawa, Y. & Oguchi, T. Superexchange interaction in the A-site ordered perovskite $YMn_3Al_4O_{12}$. *Phys. Rev. B* **92**, 014420 (2015).
7. Saito, T. et al. Symmetry-breaking 60°-spin order in the A-site-ordered perovskite $LaMn_3V_4O_{12}$. *Phys. Rev. B* **90**, 214405 (2014).

8. Ovsyannikov, S. V. et al. New antiferromagnetic perovskite $CaCo_3V_4O_{12}$ prepared at high-pressure and high-temperature conditions. *Inorg. Chem.* **52**, 11703–11710 (2013).

9. Ovsyannikov, S. V. et al. Structural and magnetic transitions in $CaCo_3V_4O_{12}$ perovskite at extreme conditions. *Inorg. Chem.* **56**, 6251–6263 (2017).

10. Amano Patino, M. et al. Multi-*k* spin ordering in $CaFe_3Ti_4O_{12}$ stabilized by spin-orbit coupling and further-neighbor exchange. *Phys. Rev. Res.* **3**, 043208 (2021).

11. Shiraki, H. et al. Ferromagnetic cuprates $CaCu_3Ge_4O_{12}$ and $CaCu_3Sn_4O_{12}$ with A-site ordered perovskite structure. *Phys. Rev. B* **76**, 140403 (2007).

12. Brese, N. E. & O'Keeffe, M. Bond-valence parameters for solids. *Acta Crystallogr. Section B Struct. Sci.* **47**, 192–197 (1991).

13. Koo, H.-J., Xiang, H. J., Lee, C. & Whangbo, M.-H. Effect of magnetic dipole−dipole interactions on the spin orientation and magnetic ordering of the spin-ladder compound $Sr_3Fe_2O_5$. *Inorg. Chem.* **48**, 9051–9053 (2009).

14. Koo, H.-J. & Whangbo, M.-H. Spin exchange and magnetic dipole–dipole Interactions leading to the magnetic superstructures of MAs_2O_6 (M = Mn, Co, Ni). *Inorg. Chem.* **53**, 3812–3817 (2014).

15. Xiang, H. J., Lee, C., Koo, H.-J., Gong, X. & Whangbo, M.-H. Magnetic properties and energy-mapping analysis. *Dalton Trans.* **42**, 823–853 (2012).

16. Whangbo, M. H. & Xiang, H. *Handbook of Solid State Chemistry,* Vol. 5, 285–343 (John Wiley & Sons, 2017).

17. Li, X. et al. Spin Hamiltonians in magnets: Theories and computations. *Molecules* **26**, 803 (2021).

18. Moriya, T. Anisotropic superexchange interaction and weak ferromagnetism. *Phys. Rev.* **120**, 91–98 (1960).

19. Blöchl, P. E. Projector augmented-wave method. *Phys. Rev. B* **50**, 17953–17979 (1994).

20. Kresse, G. & Joubert, D. From ultrasoft pseudopotentials to the projector augmented-wave method. *Phys. Rev. B* **59**, 1758–1775 (1999).

21. Kresse, G. & Furthmüller, J. Efficient iterative schemes for ab initio total-energy calculations using a plane-wave basis set. *Phys. Rev. B* **54**, 11169–11186 (1996).

22. Perdew, J. P., Burke, K. & Ernzerhof, M. Generalized gradient approximation made simple. *Phys. Rev. Lett.* **77**, 3865–3868 (1996).

23. Dudarev, S. L., Botton, G. A., Savrasov, S. Y., Humphreys, C. J. & Sutton, A. P. Electron-energy-loss spectra and the structural stability of nickel oxide: An LSDA+U study. *Phys. Rev. B* **57**, 1505–1509 (1998).

24. Toyoda, M., Yamauchi, K. & Oguchi, T. Ab initio study of magnetic coupling in $CaCu_3B_4O_{12}$ (B= Ge, Zr, and Sn). *Phys. Rev. B* **87**, 224430 (2013).

25. Rhee, H. B. & Pickett, W. E. Strong interactions, narrow bands, and dominant spin-orbit coupling in Mott insulating quadruple perovskite $CaCo_3V_4O_{12}$. *Phys. Rev. B* **90**, 205119 (2014).

26. Whangbo, M.-H., Canadell, E., Foury, P. & Pouget, J.-P. Hidden Fermi surface nesting and charge density wave instability in low-dimensional metals. *Science* **252**, 96–98 (1991).

27. Avdeev, M. & Hester, J. R. ECHIDNA: A decade of high-resolution neutron powder diffraction at OPAL. *J. Appl. Crystallogr.* **51**, 1597–1604 (2018).

28. Toby, B. H. & Von Dreele, R. B. GSAS-II: The genesis of a modern open-source all purpose crystallography software package. *J. Appl. Crystallogr.* **46**, 544–549 (2013).

29. Perez-Mato, J. M. et al. Symmetry-based computational tools for magnetic crystallography. *Annu. Rev. Mater. Res.* **45**, 217–248 (2015).

30. Kuneš, J., Novák, P., Schmid, R., Blaha, P. & Schwarz, K. Electronic structure of fcc Th: Spin-orbit calculation with $6p_{1/2}$ local orbital extension. *Phys. Rev. B* **64**, 153102 (2001).

Author contributions

The study was designed by M.A.P., F.D.R., and Y.S. Sample synthesis was carried out by M.A.P., F.D.R. and Y.S. Structural and physical property characterisation was performed by M.A.P. and F.D.R. with contributions from S.D.I. and M.G. M.A. collected neutron powder diffraction data and analysis of these was carried out by M.A.P. and F.D.R. DFT calculations were carried out and analyzed by H.-J.K. and M.-H.W. to find the role of the underlying kagome lattice. The manuscript was written with contributions from all authors.

Competing interests

The authors declare no competing interests.

Additional information

Supplementary information The online version contains supplementary material available at https://doi.org/10.1038/s43246-022-00274-y.

Correspondence and requests for materials should be addressed to Fabio Denis Romero, Hyun-Joo Koo or Yuichi Shimakawa.

Peer review information *Communications Materials* thanks the anonymous reviewers for their contribution to the peer review of this work. Primary Handling Editors: Alannah Hallas and Aldo Isidori.

Reprints and permission information is available at http://www.nature.com/reprints

Publisher's note Springer Nature remains neutral with regard to jurisdictional claims in published maps and institutional affiliations.